

# Wide-Band Nonreciprocity of Surface Acoustic Waves Induced by Magnetoelastic Coupling with a Synthetic Antiferromagnet

Roman Verba<sup>1,\*</sup>, Vasil Tiberkevich,<sup>2</sup> and Andrei Slavin<sup>2</sup>

<sup>1</sup> Institute of Magnetism, Kyiv 03142, Ukraine

<sup>2</sup> Department of Physics, Oakland University, Rochester, Michigan 48309, USA

(Received 20 August 2019; revised manuscript received 1 October 2019; published 26 November 2019)

Nonreciprocal propagation of acoustic waves is often achieved by magnetoelastic coupling with spin waves (SWs) and is limited to a narrow magnetoelastic gap (approximately 10–100 MHz) near the crossing point of the acoustic and SW dispersions. We propose a different method to achieve a giant frequency band of the surface acoustic wave (SAW) nonreciprocity in an artificial structure, where a nonmagnetic acoustic crystal is magnetoelastically coupled to a synthetic antiferromagnet—a pair of thin ferromagnetic layers the static magnetizations of which are held opposite by Ruderman-Kittel-Kasuya-Yoshida interaction. Strongly nonreciprocal and approximately *linear* dispersion of SWs in this system makes it possible to match dispersions of SAWs and SWs in a wide frequency band for one direction of the wave propagation. Example calculations performed for the LiNbO<sub>3</sub>/Co/Ru/Co structure confirm the giant nonreciprocity of the SAW propagation in a frequency band exceeding 6 GHz.

DOI: 10.1103/PhysRevApplied.12.054061

## I. INTRODUCTION

Wave nonreciprocity—the dependence of the wave-propagation characteristics (the dispersion and/or the damping rate) on the reversal of the propagation direction—is a fascinating fundamental phenomenon, which is also of great practical interest for the development of isolators and circulators. The existence of wave nonreciprocity requires a simultaneous breaking of the time- and space-reversal symmetries [1–3], which is difficult to realize in both natural and artificial materials. In particular, the symmetry of the fundamental laws of mechanics prohibits the nonreciprocity of pure acoustic waves (AWs) in unmoving media. Nonreciprocal propagation of AWs can be realized in the presence of moving or rotating media [4,5] or by utilizing time-reversal-breaking nonlinear effects [6–8], all of which have severe limitations for practical applications. Wave propagation in diffractive media could also appear as unidirectional [9] but, in fact, is neither nonreciprocal nor useful for applications [10].

Alternatively, nonreciprocal propagation of AWs can be induced by interaction with other subsystems of a medium [11]. Usually, one considers magnetoelastic interaction with a magnetic subsystem of a ferromagnetic crystal as a source of acoustic nonreciprocity [12–14]. Indeed, the time-reversal symmetry of the magnetic moment motion is inherently broken—its natural precession is always right-handed. The lack of inversion symmetry in

magnetic crystals [15,16] or in artificial structures [17–19] allows one to realize the nonreciprocity of spin excitations—spin waves (SWs)—in many different cases.

A schematic illustration of the nonreciprocal propagation of AWs, induced by magnetoelastic coupling with SWs, is given in Fig. 1. In the simplest and most well-studied case [Fig. 1(a)], the AWs and SWs themselves (i.e., without magnetoelastic coupling) are reciprocal and both the wave dispersion and the propagation losses are the same for opposite propagation directions. In the vicinity of the crossing points of the AW and SW dispersion characteristics, magnetoelastic interaction leads to the coupling between these waves and to the opening of magnetoelastic gaps (the effect of wave hybridization or “avoided crossing”). The main experimental manifestation of this coupling is the increased damping (decreased transmission rate) of the AWs near the gaps, caused by the magnetic losses, which are usually much larger than the acoustic ones. Since the size of the magnetoelastic gap depends on the vector structure of the interacting waves, the gaps for opposite wave vectors  $\pm\mathbf{k}$  may be different. Consequently, the AW propagation losses at a given frequency also become different for opposite propagation directions, being, however, large in both directions (so that the relative difference in the losses is typically rather small) [14]. This simple scheme has previously been studied in ferromagnetic single crystals [12,13] and artificial structures [14].

An alternative method of inducing AW nonreciprocity has been proposed in Ref. [20]. In this case, the SWs

\*verrv@ukr.net

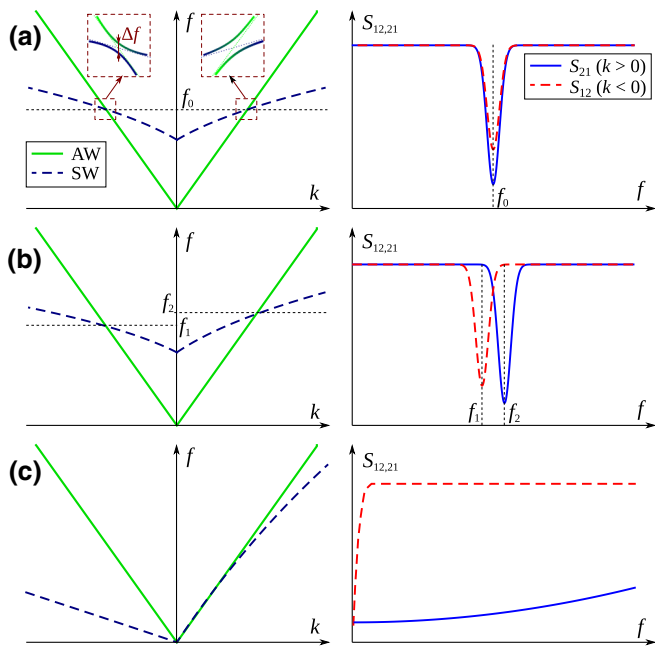


FIG. 1. An illustration of methods of inducing nonreciprocity of an AW by magnetoelastic coupling with a SW: left column, spectra of AWs and SWs—the inset in (a) shows the opening of the magnetoelastic gap of size  $\Delta f$ ; right column, AW transmission rates in opposite directions (schematically). Here, (a) and (b) show the narrow-band nonreciprocity with coinciding and frequency-separated hybridization bands, respectively, and (c) illustrates the method of creation of wide-band nonreciprocity proposed in the current work.

have inherently nonreciprocal spectra (e.g., due to the Dzyaloshinskii-Moriya interaction), which results in the frequency separation of magnetoelastic gaps for opposite propagation directions [Fig. 1(b)]. Thus, the high-damping (low-transmission) bands are also separated in frequency, which allows one to substantially decrease the insertion losses of a nonreciprocal device in one of the opposite propagation directions.

It should be noted that in both of the above-described schemes, the nonreciprocal propagation of AWs is limited to a frequency range of the order of the magnetoelastic hybridization gap  $\Delta f$  near the crossing points of the dispersion characteristics, which typically does not exceed 10–100 MHz [20]. It creates certain limitations for practical applications, such as a limited operation band and the necessity to fabricate different structures for different frequency ranges (or their fine tuning by an external magnetic field). In addition, if the magnetoelastic gaps are smaller than the SW linewidth and/or the frequency band of transducers for the AW excitation and reception (which is a common case for many magnetic and acoustic systems), the full potential of the AW nonreciprocity induced by magnetoelastic interaction cannot be realized [20].

## II. PRINCIPLE OF WIDE-BAND NONRECIPROCITY OF ACOUSTIC WAVES

In this work, we propose a method to realize wide-frequency-band AW-SW nonreciprocity. It is based on an artificial material, in which the nonreciprocal properties of AWs [specifically, the surface acoustic wave (SAW)] exist over a much wider frequency range that can exceed several gigahertz and, therefore, covers the full band of the SAW applications. The main idea is illustrated in Fig. 1(c). Namely, we propose to couple a SAW with a SW, which is strongly *nonreciprocal*, and, for one direction of propagation, has a *dispersion characteristic that is similar to that of the SAW*. In such a case, the effective coupling between the SW and the SAW takes place in a wide frequency region, where the SAW and SW dispersions are similar, instead of a relatively narrow AW-SW hybridization band near the dispersion crossing points, as in the previously used hybridized systems [see Figs. 1(a) and 1(b)].

We consider the possibility of nonreciprocal propagation of SAWs, which are the AWs that are used most often in modern signal-processing techniques [21–23]. In addition, the localization of SAWs near the crystal surface makes them sensitive to the properties of thin films adjacent to the acoustic crystal and, in particular, to ferromagnetic layers placed on the surface of a crystal [14,24]. Nevertheless, the above-described approach of induced AW-SW nonreciprocity could be used for AWs other than the SAW (e.g., Lowe's waves) through a proper choice of the adjacent magnetic structure.

The spectrum of the SAW is linear and gapless [see Fig. 2(d)],  $\omega_{\text{SAW}} = c_{\text{SAW}}|k|$ , where  $c_{\text{SAW}}$  is the SAW velocity. Therefore, for the realization of the proposed approach of wide-band nonreciprocity, one needs to find a ferromagnetic structure in which the SW spectrum is *nonreciprocal*, *gapless*, and *linear* (at least, over a certain range of wave numbers). The structure that satisfies these requirements is a synthetic antiferromagnet—a ferromagnetic bilayer with opposite directions of the static magnetization of layers, which can be stabilized by Ruderman-Kittel-Kasuya-Yoshida (RKKY) indirect exchange via a spacer of a proper thickness. The SW spectrum of a synthetic antiferromagnet consists of two branches having different phase relations between the magnetization precession in the layers [Fig. 2(c)] and a set of higher-frequency nonuniform-thickness modes [not shown in Fig. 2(c)]. Both SW branches are strongly *nonreciprocal* as long as the static magnetization of the layers lies in plane (or has a nonzero in-plane component) and the SW propagates in plane at a finite angle to the static magnetization, i.e.,  $\phi \neq 0, \pi$  [see Fig. 2(a)] [25,26]. In the ideal case of identical layers and a zero external field, the lowest SW branch is gapless and, at sufficiently small values of the SW wave number  $k$ , has linear dispersion. These spectral properties of SWs in a synthetic antiferromagnet are exactly the

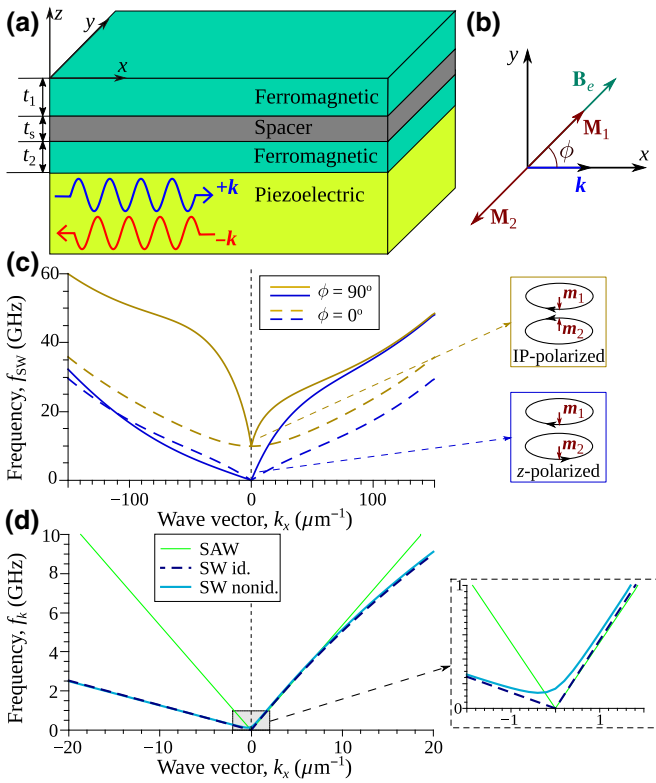


FIG. 2. (a) The layout of the proposed artificial structure. (b) The directions of the wave propagation, the bias field, and the magnetizations of the ferromagnetic layers in the  $x$ - $y$  plane. (c) The SW spectra of the synthetic antiferromagnet in the case of identical layers in a zero bias field [Co(15)/Ru(0.9)/Co(15), thicknesses in nanometers] for different SW propagation directions. (d) The dispersion of the lowest SW branch at  $\phi = 36^\circ$  in the ideal case of identical magnetic layers in a zero bias field (dashed line) and in the case of slightly different magnetic layers [Co(16)/Ru(0.9)/Co(15)] in a  $B_e = 1$  mT bias field. The green line shows the spectrum of the SAW in LiNbO<sub>3</sub>. Details of the spectral calculation are presented in the Appendix.

properties that are needed to match the spectral properties of SAWs.

### III. CALCULATION OF WAVE SPECTRA AND PROPAGATION LOSSES

The layout of a structure in which the above-described nonreciprocal SWs can be efficiently coupled with a SAW is shown in Fig. 2(a). It consists of a nonmagnetic acoustic single crystal that supports propagation of the SAW (e.g., LiNbO<sub>3</sub>, LiTiO<sub>3</sub>, etc.) and the adjacent thin synthetic antiferromagnet that has magnetostrictive ferromagnetic layers. If the ferromagnetic layers are thin compared to the SAW localization depth (of the order of the SAW wavelength), their presence hardly affects the SAW mechanically. The strain induced by the SAW penetrates freely into the magnetic layers, where it couples to SWs due to the magnetostriction effect.

In all the calculations below, we use the parameters of a Co/Ru/Co/LiNbO<sub>3</sub> structure, with Co being in the fcc or bcc phase; notes on the choice of materials are presented below (Sec. IV). Namely, we use the following parameters: saturation magnetization of Co  $\mu_0 M_s = 1.76$  T, gyromagnetic ratio  $\gamma = 2\pi \times 29$  GHz/T [27], exchange stiffness  $A_{ex} = 2.5 \times 10^{-11}$  J/m [28], and Gilbert damping constant  $\alpha_G = 0.006$  [29]. The thickness of the Ru spacer, which corresponds to a local maximum of the RKKY antiferromagnetic exchange, is chosen to be  $t_s = 0.9$  nm. The corresponding constant of the antiferromagnetic interlayer exchange is  $J = 0.8$  mJ/m<sup>2</sup> [30]. The magnetoelastic coupling constants of Co are  $B_1 = -9.2$  MJ/m<sup>3</sup>,  $B_2 = 7.7$  MJ/m<sup>3</sup> [31,32]. The parameters of the LiNbO<sub>3</sub> are as follows: Y-cut, Z-propagation axis of SAW, density  $\rho = 4650$  kg/m<sup>3</sup>, longitudinal and transversal sound velocities  $c_l = 7350$  m/s and  $c_t = 3600$  m/s [33], respectively, and corresponding SAW velocity  $c_{SAW} = 3361$  m/s.

SW dispersion in a synthetic antiferromagnet has been considered in Refs. [25] and [26]. In the case of identical ferromagnetic layers and a zero external bias field, the long-wave (small  $k$ ) approximation of the lowest SW branch yields the following dispersion relation:

$$\omega_{\mathbf{k}} = \omega_M t_{FM} \left[ \sqrt{\frac{\lambda^2}{t_{FM}^2} + \frac{1}{3} \sin^2 \phi + \frac{1}{2} \sin \phi \operatorname{sign} k} \right] |k|, \quad (1)$$

where  $\omega_M = \gamma \mu_0 M_s$ ,  $M_s$  is the saturation magnetization,  $t_{FM} = t_1 = t_2$  is the thickness of the ferromagnetic layers, and  $\lambda$  is the exchange length. It is clear that this dispersion is *gapless*,  $\omega_0 = 0$ , which reflects the continuous rotational symmetry in the plane of the layers. The SW spectrum is also *linear*,  $\omega_{\mathbf{k}} = c_\phi |k|$ , with the velocity  $c_\phi$  dependent on the angle  $\phi$  of SW propagation relative to the static magnetization. Finally, the SW spectrum is *nonreciprocal*,  $\omega_{\mathbf{k}} \neq \omega_{-\mathbf{k}}$  (except for  $\phi = 0$ ). The angular dependence of the SW velocity  $c_\phi$  greatly simplifies the design of the artificial structure, as it allows one to easily match the group velocities of SW and SAW,  $c_\phi \approx c_{SAW}$ , by the selection of a proper propagation angle  $\phi$  (see below). The linearity of the SW dispersion holds up until  $|k| \ll 1/h, 1/\lambda$ . At higher wave numbers, the SW dispersion deviates from the linear law, as shown in Fig. 2(d).

In practice, one cannot use this idealized case, since the continuous degeneracy of the magnetic state does not allow one to fix the angle between the  $\mathbf{k}$  and  $\mathbf{M}$ —it will fluctuate under thermal noise. A possible solution is to use slightly different ferromagnetic layers (in saturation magnetization  $M_i$  and/or in thickness  $t_i$ ) and apply a weak in-plane magnetic field  $\mathbf{B}_e$ . If the bias field does not exceed the critical value  $|B_e| < J |(M_2 t_2)^{-1} - (M_1 t_1)^{-1}|$  (see the Appendix), where  $J$  is the constant of the interlayer antiferromagnetic exchange (RKKY), the antiferromagnetic state

remains stable and the magnetizations of the layer align with the direction of the bias field  $\mathbf{B}_e$ , so that the net magnetic moment of the bilayer is parallel to  $\mathbf{B}_e$ . Alternatively, one can utilize a weak in-plane anisotropy caused by the crystal structure of the ferromagnetic material or by the sample shape (see the notes on acceptable anisotropy values in Sec. IV). This in-plane anisotropy would create the same stabilizing effect as the in-plane bias magnetic field. The presence of a weak magnetic field or anisotropy does not drastically change the SW spectrum. It leads to the appearance of a small spectral gap,  $\omega_0 > 0$ , but, apart from a small region near  $k = 0$ , the SW spectrum still follows the linear law [see Fig. 2(d)].

The coupling between the SW and the SAW is calculated using the perturbation approach developed in Ref. [20]. The coupling coefficient is as follows:

$$\kappa_k = \frac{2 \cos \phi}{\sqrt{A_k Q_k}} \int \mu(z) [B_1 u_{xx} m_{IP}^* \sin \phi + B_2 u_{xz} m_z^*] dz. \quad (2)$$

Here,  $\mu(z)$  defines the direction of static magnetization of the layers relative to the direction of the bias field [i.e.,  $\mu = 1$  within the upper (thicker) layer and  $\mu = -1$  within the lower layer; otherwise,  $\mu = 0$ ],  $m_{IP}(z)$  and  $m_z(z)$  are the in-plane and out-of-plane components of the dynamic magnetization in the SW mode,  $\hat{\mathbf{u}}(z)$  is the strain tensor of the SAW, and  $B_1$  and  $B_2$  are the coefficients of the magnetoelastic coupling tensor. Finally,  $A_k$  and  $Q_k$  are the normalization constants of the SW and the SAW (see the Appendix).

In the vicinity of the surface, the components of the SAW strain tensor satisfy the condition  $|u_{xz}| \ll |u_{xx}|$ , so that the coupling strength is mainly determined by the first term in the brackets, which is proportional to  $\sin(2\phi)\mu(z)m_{IP}^*(z)$ . For the lowest SW mode, the in-plane components of the dynamic magnetization in the layers are in opposite phases,  $m_{IP,1} = -m_{IP,2}$  [see Fig. 2(c)]. Since

$\mu_1 = -\mu_2$ , it is clear that the contributions from the two layers have the same sign and enhance each other. Thus, both layers can be made from the same ferromagnetic material, i.e., have the same magnetostriction. In contrast, for the coupling of the SAW to the higher SW mode, the synthetic antiferromagnet should be asymmetric in magnetostriction, e.g., one layer should not be magnetostrictive at all.

The magnetoelastic coupling between the SW and the SAW is a maximum at the magnetization angle  $\phi \approx 45^\circ$  for a fixed layer thickness, as is common for interactions of SAWs with thin ferromagnetic layers [14,24]. Also, the coupling is, as expected, proportional to the thickness  $t_i$  of the layers (at a given  $\phi$ ), as with the increase of  $t_i$  the overlapping volume of the SW and the SAW is increased. If the layer thickness increases, the match of the SW and SAW dispersion happens at a smaller angle  $\phi$ , because the SW velocity  $c_\phi$  is proportional to the layer thickness. In general, an increase of the layer thickness with a simultaneous decrease of the angle  $\phi$  (to satisfy the matching condition  $c_\phi \approx c_{SAW}$ ) leads to a small increase of the coupling strength. However, one should be aware that a large thickness of the ferromagnetic layers reduces the range of linearity of the SW dispersion, which extends until  $kt_i \ll 1$ . Thus, the optimal thickness of the ferromagnetic layers is determined by an interplay between the desirable strength of nonreciprocity (proportional to the coupling) and the size of the nonreciprocal frequency band (the range of linearity of the SW dispersion) and will be different for different possible applications.

In Fig. 3, we present the calculated characteristics of the Co(16)/Ru(0.9)/Co(15)/LiNbO<sub>3</sub> artificial structure. For this structure, the match of the SW and SAW dispersion characteristics takes place at the angle  $\phi = 36^\circ$ . It is clear from Fig. 3(a) that the distance between the SW and SAW frequencies in the positive propagation direction ( $k_x > 0$ ) is smaller than, or comparable to, the coupling rate  $\kappa$  over a wide range of wave numbers, meaning that

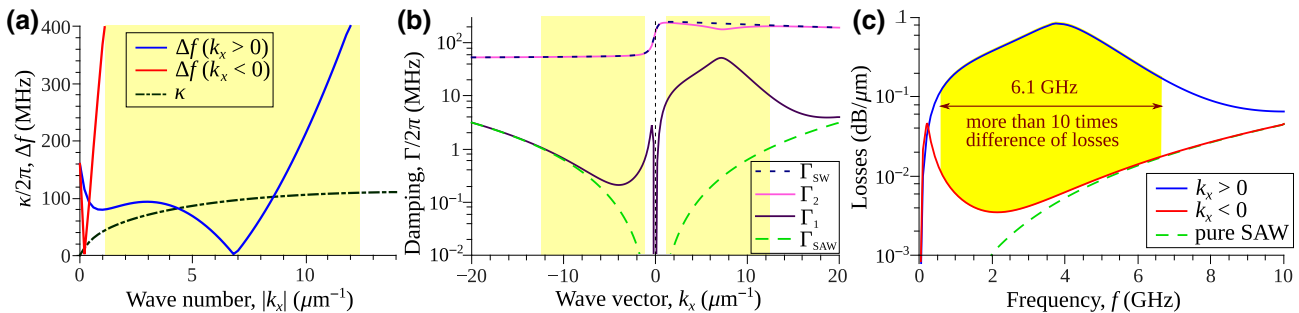


FIG. 3. (a) The frequency distance between the dispersion branches of the uncoupled SAW and SW and the coupling strength  $\kappa$  as functions of the wave number. (b) The damping rates of coupled magnetoelastic waves ( $\Gamma_1$  and  $\Gamma_2$ ) and uncoupled SW ( $\Gamma_{SW}$ ) and SAW ( $\Gamma_{SAW}$ ). (c) The frequency dependence of the propagation losses of the SAW, coupled to the SW, in opposite propagation directions. The yellow shaded area in all panels shows the same region, where the propagation losses for the opposite propagation directions differ by a factor of 10 or more. The calculations are made for Co(16)/Ru(0.9)/Co(15)/LiNbO<sub>3</sub>,  $B_e = 1$  mT,  $\phi = 36^\circ$ .

the magnetic layers have a strong influence on the SAW propagation within all of this frequency range. In contrast, for the negative propagation direction, the frequency distance between the SW and SAW dispersion branches is much larger than the coupling and the SW and SAW propagate almost independent of each other.

The magnetoelastic coupling between the SAW and the SW leads to the formation of hybrid magnetoelastic waves. Their frequencies  $\omega_{1,2}$  and damping rates  $\Gamma_{1,2}$  are determined by the standard relation for coupled waves, namely

$$\begin{aligned} \omega_{1,2} - i\Gamma_{1,2} \\ = \frac{\omega_{\text{SW}} - i\Gamma_{\text{SW}} + \omega_{\text{SAW}} - i\Gamma_{\text{SAW}}}{2} \\ \pm \sqrt{\left[ \frac{(\omega_{\text{SW}} - i\Gamma_{\text{SW}}) - (\omega_{\text{SAW}} - i\Gamma_{\text{SAW}})}{2} \right]^2 + |\kappa_k|^2}, \end{aligned} \quad (3)$$

As has been pointed out earlier, the coupling significantly affects the damping rates of the SAW, since a part of the energy of a magnetoelastic wave is dissipated in the magnetic subsystem. This effect is evident from Fig. 3(b) as, for a positive propagation direction, the damping rate  $\Gamma_1$  of the coupled wave increases drastically in comparison to the damping rate of a pure SAW. In the negative propagation direction, for which the spectra of the pure SW and SAW are well separated,  $\Gamma_1$  is much smaller than for the positive propagation direction and approaches  $\Gamma_{\text{SAW}}$  much more quickly.

Transmission losses in a SAW transmission line with a synthetic antiferromagnet are mainly determined by the coupled magnetoelastic wave with lower damping rate  $\Gamma_1$ , since the second coupled wave, which has much larger damping rate  $\Gamma_2$ , decays completely (below the thermal level) at the length of a typical SAW line. In our artificial material, the variation of the damping rate  $\Gamma_1$  with the wave number is much smaller than the width of the excitation spectrum of a typical interdigital SAW transducer. This allows one to get rid of the nonresonant excitation and to realize the full potential of the SAW nonreciprocity, induced by the magnetoelastic coupling, which is impossible to achieve in other schemes [Figs. 1(a) and 1(b)]. The propagation losses can be estimated simply as  $L = 10 \log(\Gamma_1 l / v)$ , where  $v \approx c_{\text{SAW}}$  is the group velocity of the coupled wave and  $l$  is the length of the SAW transmission line. As is clear from Fig. 3(c), the propagation losses are significantly nonreciprocal in a giant frequency band. They differ by more than one order of magnitude for opposite propagation directions in the frequency range of 6.1 GHz (from 0.6 to 6.6 GHz). This giant frequency band of the SAW nonreciprocity is almost 100 times wider than the nonreciprocity regions that can be obtained using

the traditional methods with a pointlike spectral crossing. It is important to note that this giant frequency band of the SAW nonreciprocity covers almost all the range of the possible SAW applications in microwave signal processing [21].

It is also important to note that the effect of the wide-band SAW nonreciprocity is quite robust with respect to the angle  $\phi$  between the static magnetization and the wave-propagation direction and that perfect alignment of the magnetization direction is not necessary for the experimental observation and utilization of the effect. For example, a decrease of the angle  $\phi$  by 5° results in the reduction of the highly nonreciprocal frequency range (highlighted in Fig. 3) to 4.5 GHz. Moreover, a moderate increase of this angle does not lead to a reduction of the nonreciprocity range but only to a more complex dependence of the propagation losses within it; a significant reduction takes place only at  $\phi > 45^\circ$ .

#### IV. NOTES ON MATERIAL CHOICE

In this section, we briefly discuss the requirements for the ferromagnetic material in the synthetic antiferromagnet multilayer, which should be satisfied for the realization of wide-band nonreciprocity of SAW. Naturally, as is usual for magnetoelastic devices, the requirements of a high magnetostriction and sufficiently low magnetic damping (if the magnetic damping significantly exceeds the magnetoelastic coupling  $\kappa$ , the SAW and SW become effectively uncoupled) [20] hold in our case too. The specific requirements follow from Eqs. (1) and (2). The SW group velocity is proportional to the saturation magnetization and the layer thickness. It is clear that the maximal value of the group velocity, which is realized at  $\phi = 90^\circ$ , should be larger than the SAW velocity, maintaining, simultaneously, a reasonably small bilayer thickness in order to not significantly affect the SAW propagation mechanically. The SAW velocity in LiNbO<sub>3</sub> is quite high,  $c_{\text{SAW}} = 3361$  m/s, so the saturation magnetization of the ferromagnetic should be sufficiently high too. In particular, nickel, which is commonly used as a magnetostrictive material, is not a good choice in combination with LiNbO<sub>3</sub> due to its relatively low static magnetization  $M_s$ . If Ni is used as a ferromagnetic material, the thicknesses of the ferromagnetic layers should exceed 40 nm each to match the SAW dispersion. Instead, Co, Fe, or CoFe alloys are suitable magnetic materials in combination with LiNbO<sub>3</sub>. The use of acoustic crystals that have slower SAWs increases the variety of acceptable ferromagnetic materials.

Another important requirement concerns the anisotropy of the ferromagnetic layers. It is desirable to have vanishing anisotropy in the plane of the layers. The presence of anisotropy sufficiently increases the SW spectrum gap (frequency at  $k = 0$ ) and it becomes impossible to match the

SW and SAW dispersions at low frequencies. The sensitivity of the SW spectrum gap to the anisotropy field is much higher than to the external field, since the anisotropy has the same effect in both layers (increase of the frequency), while the external field acts oppositely. For example, an in-plane anisotropy of 2 mT in the studied structure increases the SW spectrum gap to  $\omega_0 = 1.7$  GHz and reduces the range over which the SAW propagation losses differ by at least a factor of 10 (shown in Fig. 3) from 6.1 GHz to 4 GHz (range 3.3 to 7.3 GHz). An in-plane anisotropy of 5 mT or more leads to a standard dispersion crossing [shown in exemplary form in Fig. 1(b)] instead of the dispersion matching necessary for wide-band nonreciprocity. Thus, if one uses in-plane anisotropy for the stabilization of the magnetization state instead of an external field, the anisotropy should be really weak, characterized by an effective anisotropy field below 1 mT. Simultaneously, perpendicular magnetic anisotropy does not have such a critical impact. It simply reduces the SW group velocity; this reduction can be roughly estimated by the substitution  $\omega_M \rightarrow (\omega_M - 2\gamma K_\perp/M_s)$ , where  $K_\perp$  is the constant of the perpendicular anisotropy.

If it is impossible to get rid of a relatively high in-plane anisotropy in the fabrication process, its undesirable effect can be eliminated by the simultaneous application of a sufficient in-plane magnetic field. Indeed, a sufficient bias field results in the instability of the antiferromagnetic state and in-plane anisotropy simply increases this critical value compared to the isotropic case [Eq. (A10)]. Near this point, the SW spectrum gap is vanishingly small and the SW spectrum can approximately fit the SAW dispersion, although it becomes more complex than the linear spectrum in the isotropic case [Eq. (1)].

## V. CONCLUSIONS

In summary, we demonstrate a way to realize nonreciprocal propagation of a SAW in a giant frequency band by coupling of the SAW to the SWs in a synthetic antiferromagnet that has magnetostrictive ferromagnetic layers. In the proposed approach, the SW spectrum is nonreciprocal and is similar to the SAW spectrum: it has a small spectral gap and it is approximately linear over a wide frequency range. These features lead to the coalescence of the SW and SAW spectra for one propagation direction, making magnetoelastic interaction between these waves very efficient over a wide frequency band, which could exceed several gigahertz. This efficient magnetoelastic interaction leads to increased losses of SAWs due to the energy dissipation in the magnetic subsystem. The calculations for a Co/Ru/Co/LiNbO<sub>3</sub> structure, presented as an example, demonstrate a large nonreciprocity of the SAW propagation losses in the frequency band exceeding 6 GHz. We believe that our results open a way for the development of a new generation of wide-band nonreciprocal SAW devices.

## ACKNOWLEDGMENTS

This work was supported in part by the U.S. National Science Foundation (Grants No. EFMA-1641989 and No. ECCS-1708982), by the Oakland University Foundation, and by the Ministry of Education and Sciences of Ukraine (project No. 0118U004007).

## APPENDIX: CALCULATION OF SPIN-WAVE SPECTRUM OF SYNTHETIC ANTIFERROMAGNET

The spectrum and spatial profile of SWs in a synthetic antiferromagnet can be found, as usual, by solving the linearized Landau-Lifshitz equation [26,34]:

$$-i\omega_k \mathbf{m}_{k,i} = \sum_{j=1,2} \boldsymbol{\mu}_j \times \hat{\boldsymbol{\Omega}}_{ij} \cdot \mathbf{m}_{j,k}. \quad (\text{A1})$$

Here,  $\omega_k$  is the SW frequency,  $k = k_x$  is the SW wave vector, assumed to be aligned with the  $x$  axis [see Fig. 2(a) in the main text],  $\boldsymbol{\mu}_1 = -\boldsymbol{\mu}_2 = \cos\phi \mathbf{e}_x + \sin\phi \mathbf{e}_y$  are the unit vectors of the static magnetizations in the ferromagnetic layers forming a synthetic antiferromagnet,  $\mathbf{M}_i = -m_{\text{IP},i} \sin\phi \mathbf{e}_x + m_{\text{IP},i} \cos\phi \mathbf{e}_y + m_z \mathbf{e}_{z,i}$  are the distributions of the dynamic magnetization (SW profile), and the index  $i = 1, 2$  denotes the ferromagnetic layers. The operator  $\hat{\boldsymbol{\Omega}}$  is defined as

$$\begin{aligned} \hat{\boldsymbol{\Omega}}_{ij} = & \left[ \omega_{H,i} + \omega_M \lambda^2 \left( k^2 - \frac{d^2}{dz^2} \right) \right] \hat{\mathbf{I}} \Delta_{ij} \\ & + \omega_M \int dz' \hat{\mathbf{G}}_k(z - z'), \end{aligned} \quad (\text{A2})$$

where  $\omega_{H,(1,2)} = \pm\gamma B_e$  is proportional to the static internal magnetic field  $B_e$  in the layers,  $\omega_M = \gamma \mu_0 M_s$ ,  $\lambda$  is the exchange length of the ferromagnetic material,  $\Delta_{ij}$  is the Kronecker delta, and  $\hat{\mathbf{I}}$  is the unit matrix. The kernel  $\hat{\mathbf{G}}_k$  of the integral in (A2) is the magnetostatic Green's function for a ferromagnetic film [34]:

$$\hat{\mathbf{G}}_k = \begin{pmatrix} G_{xx} & 0 & G_{xz} \\ 0 & 0 & 0 \\ G_{xz} & 0 & \delta(z - z') - G_{xx} \end{pmatrix}, \quad (\text{A3})$$

where  $G_{xx} = (|k|/2) \exp[-|k(z - z')|]$  and  $G_{xz} = (ik \operatorname{sign}[z - z'])/2 \exp[-|k(z - z')|]$ .

Equation (A1), which contains the exchange differential operator of the second order, should be accompanied by the corresponding boundary conditions for the dynamic magnetization. At the outer surfaces of the ferromagnetic layers

$z_i^{(o)}$ , these conditions are

$$\pm \frac{d\mathbf{m}_i}{dz} - d_z m_z \mathbf{e}_z \Big|_{z_i^{(o)}} = 0, \quad (\text{A4})$$

while at the inner surfaces  $z_i^{(i)}$  these conditions have the form

$$\pm \frac{d\mathbf{m}_i}{dz} - d_z m_z \mathbf{e}_z \Big|_{z_i^{(i)}} - \frac{J}{\mu_0 M_s^2} \left( \mathbf{m}_i|_{z_i^{(i)}} - \mathbf{m}_j|_{z_j^{(i)}} \right) = 0. \quad (\text{A5})$$

The + and – signs in the boundary conditions correspond to the upper and lower surfaces of the ferromagnetic layers and  $d_z = K_s/(2\mu_0 M_s^2)$  is the standard pinning parameter determined by the surface anisotropy  $K_s$ , while  $J$  is the constant of the antiferromagnetic RKKY coupling. All the SW spectra presented in the main text are calculated as numerical solutions of Eq. (A1). The SW norm  $A_k$  is calculated, using numerical SW profiles, as

$$A_k = i \frac{M_s}{\gamma} \int \mathbf{m}_k^*(z) \cdot \boldsymbol{\mu}(z) \times \mathbf{m}_k(z) dz. \quad (\text{A6})$$

The normalization constant  $Q_k$  of the SAW, mentioned in Eq. (2), is equal to [20]

$$Q_k = 2\omega_k \rho \int \boldsymbol{\xi}_k^*(z) \cdot \hat{\mathbf{u}}(z) dz, \quad (\text{A7})$$

where  $\boldsymbol{\xi}(z)$  and  $\hat{\mathbf{u}}(z)$  are the profile (displacement) and strain tensor of the SAW [35] and  $\rho$  is the density of the acoustic crystal.

The analytical dispersion equation (1) obtained in the long-wave approximation and presented in the main text is derived under the following assumptions: there is a zero external bias field, the antiferromagnetic coupling between the ferromagnetic layers is neglected, and the ferromagnetic layers are identical, thin ( $k t_i \ll 1$ ), and have negligible surface anisotropy, so that the thickness distribution of the dynamic magnetization in both layers is assumed to be uniform.

For the derivation of the condition of stability of the synthetic antiferromagnet under the applied external bias field, we calculate the frequency of the lowest SW branch at  $k = 0$ , which is the lowest frequency in all the SW spectrum. The only approximation in this calculation is the assumption of a uniform dynamic magnetization distribution along the thickness of the layers, which is valid for  $k = 0$  for thin layers and/or weak surface anisotropy. The

calculated SW frequency at  $k = 0$  is as follows:

$$\begin{aligned} \omega_0^2 = & \frac{\omega_{\perp 1}^2 + \omega_{\perp 2}^2}{2} - \omega_{J1}\omega_{J2} - \left[ (\omega_{\perp 1}^2 - \omega_{\perp 2}^2)^2 / 4 \right. \\ & + \omega_{J1}\omega_{J2}(\omega_{M1} + \omega_{H1} - \omega_{H2}) \\ & \left. \times (\omega_{M2} + \omega_{H2} - \omega_{H1}) \right]^{1/2}, \end{aligned} \quad (\text{A8})$$

where  $\omega_{\perp i} = \omega_{Hi} + \omega_{Mi}$ ,  $\omega_{H1} = \gamma B_e + \omega_{J1}$ ,  $\omega_{H2} = -\gamma B_e + \omega_{J2}$ , and  $\omega_{ji} = \gamma J/(M_{s,i} t_i)$ . This frequency is real ( $\omega_0^2 \geq 0$ ) if

$$\gamma B_e (\gamma B_e + \omega_{J1} - \omega_{J2}) \leq 0, \quad (\text{A9})$$

which constitutes the condition of stability of the antiferromagnetic state. In other words, for the antiferromagnetic state to be stable, the external field should be smaller than

$$|B_e| \leq J \left| \frac{1}{M_{s,2} t_2} - \frac{1}{M_{s,1} t_1} \right|, \quad (\text{A10})$$

and the magnetization direction of the layer with a larger total magnetic moment (approximately  $M_{s,i} t_i$ ) should be aligned parallel to the bias-field direction. This condition is presented explicitly in the main text.

- [1] R. E. Camley, Nonreciprocal surface waves, *Surf. Sci. Rep.* **7**, 103 (1987).
- [2] F. D. M. Haldane and S. Raghu, Possible Realization of Directional Optical Waveguides in Photonic Crystals with Broken Time-Reversal Symmetry, *Phys. Rev. Lett.* **100**, 013904 (2008).
- [3] Z. Wang, Y. D. Chong, J. D. Joannopoulos, and M. Soljačić, Reflection-Free One-Way Edge Modes in a Gyromagnetic Photonic Crystal, *Phys. Rev. Lett.* **100**, 013905 (2008).
- [4] R. Fleury, D. L. Sounas, C. F. Sieck, M. R. Haberman, and A. Alù, Sound isolation and giant linear nonreciprocity in a compact acoustic circulator, *Science* **343**, 516 (2014).
- [5] C. P. Wiederhold, D. L. Sounas, and A. Alù, Nonreciprocal acoustic propagation and leaky-wave radiation in a waveguide with flow, *J. Acoust. Soc. Am.* **146**, 802 (2019).
- [6] M. Tanter, J.-L. Thomas, F. Coulouvrat, and M. Fink, Breaking of time reversal invariance in nonlinear acoustics, *Phys. Rev. E* **64**, 016602 (2001).
- [7] B. Liang, B. Yuan, and J.-C. Cheng, Acoustic Diode: Rectification of Acoustic Energy Flux in One-Dimensional Systems, *Phys. Rev. Lett.* **103**, 104301 (2009).
- [8] B. Liang, X. S. Guo, J. Tu, D. Zhang, and J. C. Cheng, An acoustic rectifier, *Nat. Mater.* **9**, 989 (2010).
- [9] X.-F. Li, X. Ni, L. Feng, M.-H. Lu, C. He, and Y.-F. Chen, Tunable Unidirectional Sound Propagation Through a Sonic-Crystal-Based Acoustic Diode, *Phys. Rev. Lett.* **106**, 084301 (2011).
- [10] In Ref. [9], wave propagation in the forward direction is accompanied by the transformation of the wave front. If a

- wave with this modified wave front does not pass in the return direction, it will be a nonreciprocity. Instead, only a wave with an initial (unmodified) wave front does not pass in the reverse direction.
- [11] J. Heil, B. Lüthi, and P. Thalmeier, Nonreciprocal surface-acoustic-wave propagation in aluminum, *Phys. Rev. B* **25**, 6515 (1982).
  - [12] G. Komoriya and G. Thomas, Magnetoelastic-surface waves on YIG substrate, *J. Appl. Phys.* **50**, 6459 (1979).
  - [13] Y. Shimizu, K. Hasegawas, and T. Yamada, Nonreciprocity of saw velocity on a magnetized ferrite substrate, *Electron. Comm. Jpn. Pt. I* **63**, 1 (1980).
  - [14] R. Sasaki, Y. Nii, Y. Iguchi, and Y. Onose, Nonreciprocal propagation of surface acoustic wave in Ni/LiNbO<sub>3</sub>, *Phys. Rev. B* **95**, 020407 (2017).
  - [15] R. L. Melcher, Linear Contribution to Spatial Dispersion in the Spin-Wave Spectrum of Ferromagnets, *Phys. Rev. Lett.* **30**, 125 (1973).
  - [16] D. Cortés-Ortuño and P. Landeros, Influence of the Dzyaloshinskii–Moriya interaction on the spin-wave spectra of thin films, *J. Phys.: Cond. Matter* **25**, 156001 (2013).
  - [17] J. R. Eshbach and R. W. Damon, Surface magnetostatic modes and surface spin waves, *Phys. Rev.* **118**, 1208 (1960).
  - [18] L. Udvardi and L. Szunyogh, Chiral Asymmetry of the Spin-Wave Spectra in Ultrathin Magnetic Films, *Phys. Rev. Lett.* **102**, 207204 (2009).
  - [19] R. Verba, V. Tiberkevich, E. Bankowski, T. Meitzler, G. Melkov, and A. Slavin, Conditions for the spin wave nonreciprocity in an array of dipolarly coupled magnetic nanopillars, *Appl. Phys. Lett.* **103**, 082407 (2013).
  - [20] R. Verba, I. Lisenkov, I. Krivorotov, V. Tiberkevich, and A. Slavin, Nonreciprocal Surface Acoustic Waves in Multilayers with Magnetoelastic and Interfacial Dzyaloshinskii–Moriya Interactions, *Phys. Rev. Appl.* **9**, 064014 (2018).
  - [21] D. Morgan, *Surface Acoustic Wave Filters: With Applications to Electronic Communications and Signal Processing*, Studies in Electrical and Electronic Engineering (Academic Press, London, 2010), 2nd ed.
  - [22] E. A. Ash, A. A. Oliner, G. W. Farnell, H. M. Gerard, A. A. Oliner, A. J. Slobodnik, and H. I. Smith, in *Acoustic Surface Waves*, edited by A. A. Oliner, Topics in Applied Physics (Springer, Berlin, 2014).
  - [23] P. Delsing *et al.*, The 2019 surface acoustic waves roadmap, *J. Phys. D: Appl. Phys.* **52**, 353001 (2019).
  - [24] M. Weiler, L. Dreher, C. Heeg, H. Huebl, R. Gross, M. S. Brandt, and S. T. B. Goennenwein, Elastically Driven Ferromagnetic Resonance in Nickel Thin Films, *Phys. Rev. Lett.* **106**, 117601 (2011).
  - [25] P. Grünberg, Magnetostatic spin-wave modes of a heterogeneous ferromagnetic double layer, *J. Appl. Phys.* **52**, 6824 (1981).
  - [26] S. Wintz, V. Tiberkevich, M. Weigand, J. Raabe, J. Lindner, A. Erbe, A. Slavin, and J. Fassbender, Magnetic vortex cores as tunable spin-wave emitters, *Nature Nanotech.* **11**, 948 (2016).
  - [27] X. Liu, M. M. Steiner, R. Sooryakumar, G. A. Prinz, R. F. C. Farrow, and G. Harp, Exchange stiffness, magnetization, and spin waves in cubic and hexagonal phases of cobalt, *Phys. Rev. B* **53**, 12166 (1996).
  - [28] H. F. Ding, A. K. Schmid, Dongqi Li, K. Yu. Guslienko, and S. D. Bader, Magnetic Bistability of Co Nanodots, *Phys. Rev. Lett.* **94**, 157202 (2005).
  - [29] M. Tokaç, S. A. Bunyaev, G. N. Kakazei, D. S. Schmool, D. Atkinson, and A. T. Hindmarch, Interfacial Structure Dependent Spin Mixing Conductance in Cobalt Thin Films, *Phys. Rev. Lett.* **115**, 056601 (2015).
  - [30] Y. Peng, J.-G. Zhu, and D. E. Laughlin, Interfacial Co nanolayers for enhancing interlayer exchange coupling in antiferromagnetic interlayer exchange coupling media, *J. Appl. Phys.* **91**, 7676 (2002).
  - [31] D. Sander, The correlation between mechanical stress and magnetic anisotropy in ultrathin films, *Rep. Progr. Phys.* **62**, 809 (1999).
  - [32] Z. Tian, D. Sander, and J. Kirschner, Nonlinear magnetoelastic coupling of epitaxial layers of Fe, Co, and Ni on Ir(100), *Phys. Rev. B* **79**, 024432 (2009).
  - [33] A. S. Andrushchak, B. G. Mytsyk, H. P. Laba, O. V. Yurkevych, I. M. Solskii, A. V. Kityk, and B. Sahraoui, Complete sets of elastic constants and photoelastic coefficients of pure and MgO-doped lithium niobate crystals at room temperature, *J. Appl. Phys.* **106**, 073510 (2009).
  - [34] B. A. Kalinikos and A. N. Slavin, Theory of dipole-exchange spin wave spectrum for ferromagnetic films with mixed exchange boundary conditions, *J. Phys. C: Solid State Phys.* **19**, 7013 (1986).
  - [35] L. D. Landau, L. P. Pitaevskii, A. M. Kosevich, and E. M. Lifshitz, *Theory of Elasticity*, Course of Theoretical Physics Vol. 7 (Butterworth-Heinemann, Oxford, 2012).